Methods of Earth view based calibration of the response versus scan angle of the MODIS reflective solar bands

Kevin A. Twedt,[a] Hongda Chen,[a] Xiaoxiong Xiong,[b] Amit Angal,[a] Xu Geng,[a] and Aisheng Wu[a]
[a]Science Systems and Applications Inc., Lanham, MD 20706, USA
[b]Sciences and Exploration Directorate, NASA/GSFC, Greenbelt, MD 20771, USA

ABSTRACT

The MODIS instruments on the Terra and Aqua spacecraft are cross-track scanning radiometers that view the Earth scene, a space view port, and the on-board calibrators using a two-sided scan mirror. The reflectivity of the scan mirror varies with the angle of the incident light, and changes in this response versus scan angle (RVS) need to be tracked on orbit in order to maintain accurate calibration. In this paper, we review various methods of RVS calibration of the reflective solar bands using pseudo-invariant desert targets and discuss potential advantages and disadvantages for use in future calibration.

1. INTRODUCTION

The MODIS instruments on board the Terra and Aqua spacecraft have 20 reflective solar bands (RSB) with wavelengths spanning from 412 nm to 2130 nm. MODIS is a cross-track scanning radiometer that views the Earth scene, deep space, and the on-board calibrators using a two-sided scan mirror. A reflectance-based calibration is used for the MODIS RSB, relying primarily on the observations of an on-board solar diffuser (SD). The SD views the Sun (through an optional attenuation screen) at regular intervals in order to track the on-orbit change in the gain of the MODIS detectors. The gains of the MODIS RSB, particularly the short-wavelength visible bands, have experienced significant degradation in the many years since the sensors' launches in 1999 (Terra) and 2002 (Aqua).[1–3] To maintain an accurate calibration, the calibration strategies have been updated several times on-orbit. Current methods of calibration of the MODIS RSB combine data from the SD, scheduled lunar observations, and regular observations of pseudo-invariant calibration sites (PICS) on the Earth.[4,5]

A primary component of the on-orbit gain change of the MODIS RSB is the degrading reflectance of the scan mirror. The reflectivity of the scan mirror varies with the angle of incidence (AOI) of the incident light, and this variation is referred to as the response versus scan angle (RVS). The RVS of both sides of the scan mirror was measured prior to launch for each MODIS instrument.[6] Monitoring the on-orbit changes to the RVS has been one of the most difficult challenges of MODIS calibration. The SD is only able to track the instrument's degradation at one AOI of the scan mirror, so no RVS changes can be determined from the SD measurements alone. Initial efforts to track the on-orbit RVS changes[7,8] combined the SD measurements (made at an AOI of 50.25°) with regularly scheduled lunar observations (made at an AOI of 11.2°). The MODIS instruments are also equipped with a spectroradiometric calibration assembly (SRCA) which was designed to use a set of halogen lamps to monitor on-orbit RSB gain changes at an AOI of 38.25°, but lamp failures early in the mission and subsequent operational changes mean that the SRCA cannot be used for reliable long-term calibration. Disagreement between the SD and lunar gain trends with time was interpreted as a change in the RVS of the scan mirror, and a linear interpolation of the SD and lunar results was used to model the RVS at other AOI. This on-board calibrator (OBC) based method is still used for calibration of the AOI-dependence of the gains of most MODIS RSB.

After several years of operation, it became apparent that the approach based on interpolating the SD and lunar results was no longer providing accurate calibration for some of the MODIS RSB, especially the short wavelength bands. Consequently, a new calibration approach was developed based on tracking the long term reflectance trends of North African desert PICS. The desert PICS are viewed at several different AOI of the scan mirror on a repeatable cycle. By assuming radiometric stability of these sites, the RSB gains can be determined across all AOI and time. This Earth view (EV) based method was implemented in the Collection 6 Level 1B (C6 L1B) processing of MODIS data for Terra bands 1-4, 8, and 9, and Aqua bands 8 and 9.[4,8] More recently, the C6 product also began using this method for Terra band 10,[9] and Aqua bands 1-4.[10]

The EV-based method resulted in a significant calibration improvement compared to the OBC-based method for the listed bands. But continued degradation of the MODIS instruments means that the calibration strategies must be constantly re-evaluated. For example, an alternative method of RVS calibration has been presented before[11,12] that is also based on desert PICS data, but with key differences aimed at reducing the reliance on the long-term stability of the sites. Also, the accuracy of RSB calibration across viewing angles has been tested by examining results from other pseudo-invariant targets. Deep convective clouds (DCC) have proven to be a reliable target for monitoring sensor performance and may also be used to derive the on-orbit RVS.[13–15]

In this paper, we review the history of RVS algorithms for Aqua and Terra MODIS instruments. We discuss the relative advantages of different methods of EV-based RVS calibration in an effort to develop an optimal strategy as MODIS calibration is forced to increasingly rely on Earth view targets. In section 2, we review the method used to track on-orbit changes in the RVS using on-board calibrator measurements and the limitations of this approach. In Section 3, we review the current algorithm for calibration of RVS using desert PICS, and in Section 4 we review a proposed alternative algorithm. In Section 5, we show updated results for both methods of desert-based RVS calibration, and in general the two methods show reasonably good agreement. We discuss the relative uncertainties, advantages, and disadvantages of each.

2. RVS FROM ON-BOARD CALIBRATORS

The EV reflectance factor for the MODIS RSB is defined as

$$\rho_{EV} \cos(\theta_{EV}) = dn^*_{EV} d^2_{ES} / G(t,\theta) \tag{1}$$

where dn^*_{EV} is the background and temperature corrected digital signal of each detector, d_{ES} is the Earth-Sun distance, and $G(t,\theta)$ is the time-dependent detector gain at the angle of incidence, θ, of the incident light off the scan mirror. The gain is typically written as $1/G(t,\theta) = m_1(t)/RVS(t,\theta)$, where m_1 represents the inverse of the gain at the SD AOI and RVS is a relative term that carries the AOI-dependence and is normalized to 1 at the SD AOI.

The gain at the SD AOI ($1/m_1(t)$) is calculated for all RSB, detectors, sub-frames, and scan mirror sides using the SD calibrations, the details of which have been presented before.[1,2] At the AOI of the space view (SV) port, near-monthly scheduled observations of the moon provide a reliable mechanism to monitor the instrument gain.[5] The signals from the lunar measurements, combined with a lunar irradiance model and various corrections, provide the on-orbit change in the gain at the SV AOI, $G^{oo}_{moon}(t)$. This is referenced to the initial on-orbit $m_1(t_0)$ from the SD calibration and the RVS from the pre-launch measurements, $RVS_{prl}(\theta_{SV})$, to get the absolute gain at the SV AOI:

$$\frac{1}{G(t,\theta_{SV})} = \left(\frac{m_1(t_0)}{RVS_{prl}(\theta_{SV})}\right)\frac{1}{G^{oo}_{moon}(t)} \tag{2}$$

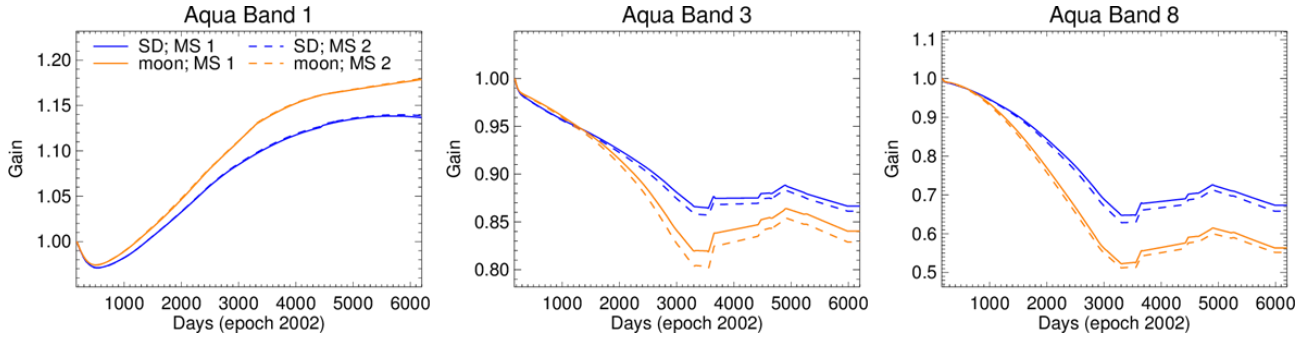

Figure 1. Mission trends of the on-orbit gain change calculated from the solar diffuser and lunar calibrations for three example bands of Aqua MODIS and both mirror sides. Deviations between the SD and lunar trends indicate on-orbit changes to the RVS.

These two calibration sources provide the baseline for MODIS RSB calibration. Figure 1 plots the on-orbit change in gain from the SD ($1/m_1^{oo}$) and the moon (G^{oo}_{moon}) for three example bands of Aqua MODIS. From early on in the mission, there are deviations between the SD and lunar trends, which indicate that the RVS of the scan mirror is changing in time. With only these two on-board measurements available, the gain at other AOI is determined from a

simple linear interpolation between the SD and lunar AOI. This calibration methodology is used in the C6 and C6.1 L1B for Terra MODIS bands 11-19 and Aqua bands 10-19 for mirror side 1. For mirror side 2, these results are modified slightly using mirror-side ratio results from nearly-uniform ocean scenes.[4] The SWIR bands 5-7 and 26 use an SD-based gain calibration but continue to use the pre-launch RVS, with no on-orbit change. For the remaining bands (Terra 1-4, 8-10 and Aqua 1-4, 8, and 9), this OBC-based method has been replaced and a method based on trends from desert PICS is used.

3. RVS FROM DESERT PICS

First, we review the desert PICS data processing. Data from three desert sites, Libya 1, Libya 2, and Libya 4, are combined to produce the gain trends. Three sites are used to reduce the dependence of the calibration on a single site and ensure good coverage across the AOI range. Views of each of these sites are recorded at up to 15 different AOI each. An overpass of each site at approximately the same AOI is made every 16 days. A few AOI from each of these three sites are chosen to calculate the gain. The sites and AOI used from each site are chosen based on the relative noise, stability, and availability of un-saturated cloud-free observations. Table 1 lists the site locations and the AOI for each site that are used in the C6 and C6.1 calibration algorithm. For convenience, we represent the AOI in terms of the frames of the MODIS EV sector. The EV sector has 1354 frames (1 km resolution) of data in one scan covering Earth viewing angles of -55° to 55° relative to nadir. The AOI on the scan mirror covers the range of 10.5° to 65.5°, giving a conversion of

$$\theta = \frac{65.5° - 10.5°}{1353} frame + 10.5° \tag{3}$$

Table 1. Summary of the desert PICS used in the two different methods of RVS calibration. This table applies to bands 1-4, 8 and 9. Terra band 10 uses a different multi-site approach due to problems with saturation early in the mission.

Method	Site	Frames (Aqua)	Frames (Terra)
C6 method	Libya 1 (+24.42°, +13.35°)	1205, 1313	111, 1329
	Libya 2 (+25.05°, +20.48°)	501, 649, 800, 939, 1055	38, 146, 225, 325, 450, 583, 745, 890
	Libya 4 (+28.55°, +23.39°)	43, 150, 228, 326, 445, 731	642, 1040, 1134
Alt-RVS method	Libya 4 (+28.55°, +23.39°)	43, 90, 150, 228, 326, 445, 584, 731, 873, 997, 1099, 1181, 1245, 1295, 1333	21, 60, 112, 179, 264, 371, 498, 642, 788, 924, 1040, 1134, 1208, 1266, 1312

For every cloud-free observation, the response of each desert site is averaged over a small area of 20 x 20 km covering each mirror side. The raw digital response is corrected for background, instrument temperature, the cosine of the solar illumination angle, and the Earth-Sun distance. This corrected digital response is denoted

$$dn_1 = \overline{\left[\frac{dn^*_{EV} d^2_{ES}}{\cos(\theta_{EV})}\right]} \tag{4}$$

where the bar indicates averaging over the pixels in the site area. Figure 2 shows examples of dn_1 trends in time for a few different AOI of Terra band 3. The dn_1 data oscillate in time because the reflectance of the desert site as viewed by the satellite depends on the bi-directional reflectance distribution function (BRDF) of the site. To reduce the oscillations, the data are further corrected to partially remove the dependence of each site's BRDF on solar illumination zenith angle (α), instrument zenith angle (ϕ), and the relative azimuth angle (ψ). A semi-empirical correction[16] is derived using the first few years of reflectance data from each AOI of each site separately. The BRDF-corrected signal is $dn_2 = dn_1 / BRDF_\theta(\alpha, \phi, \psi)$ and is also plotted in Fig. 2. The large seasonal oscillations seen at small and large AOI have been removed. We emphasize that the correction $BRDF_\theta$ is calculated and normalized separately for each AOI, due to difficulties in generating a single BRDF function that applies to all viewing angles of a site.

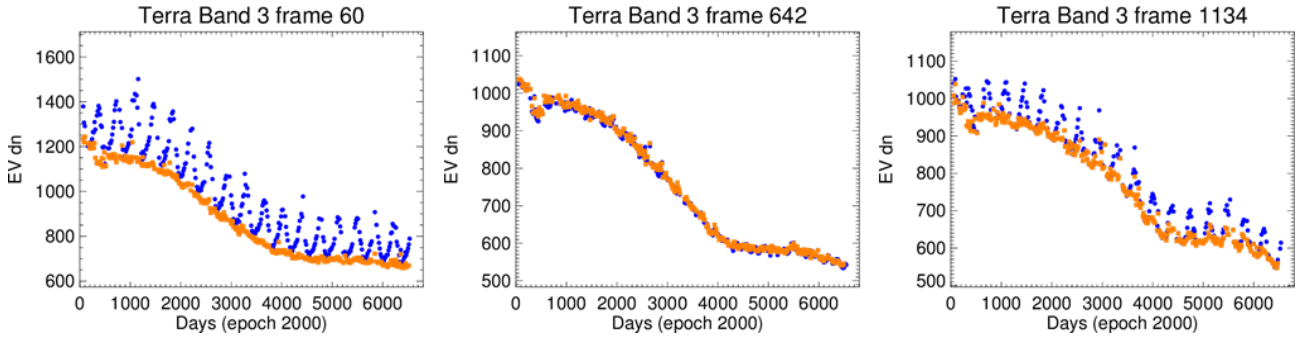

Figure 2. Signal trends of three frames of the Libya 4 site before (dn_1; blue circles) and after (dn_2; orange squares) BRDF correction for Terra band 3 mirror side 1.

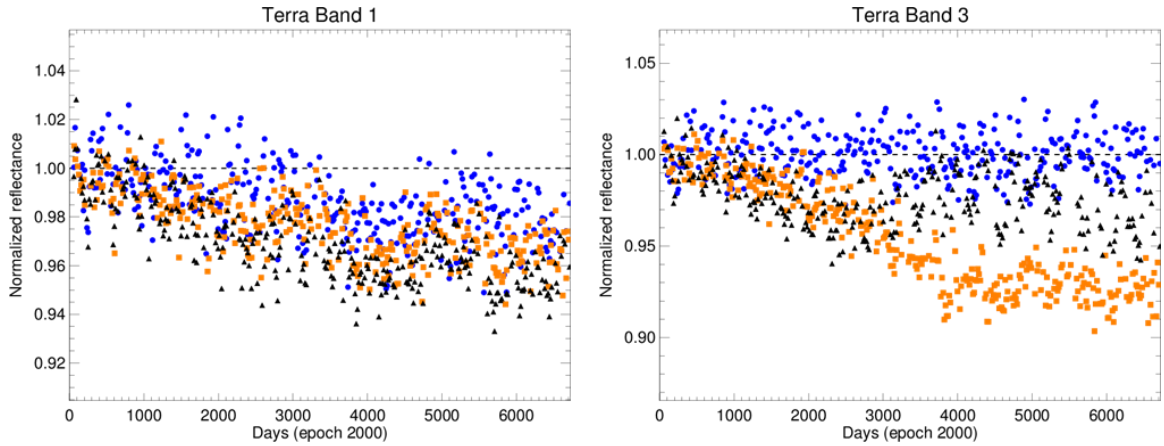

Figure 3. Trends of desert reflectance calculated using the OBC-based gain for Terra bands 1 and 3 and frames 38 (blue circles), 642 (orange squares), and 1134 (black triangles). Each trend is normalized to mission start.

After these corrections, and using Eq. 1, the reflectance of the desert sites is simply

$$\rho_{EV}(t,\theta) = dn_2/G(t,\theta) \tag{5}$$

The reflectance is still dependent on the AOI, θ, since the BRDF correction was determined separately for each AOI, but the other geometry dependencies have been removed. We can now calculate the reflectance of the desert sites using Eq. 5 and the gain derived from using the OBC-based approach described in Section 2. We expect the reflectance of these desert PICS to be constant in time at all AOI, so any deviations from unity in these trends indicate errors in the OBC-based gain. Some examples are shown in Figure 3. For bands 1 and 2 of both instruments, a deviation from unity is found for all AOI, including those near the lunar AOI. For bands 3, 4, 8, and 9 of both instruments, the OBC-based gains are in general found to be accurate near the lunar AOI, but diverge at other AOI, including the AOI of the SD, by up to 20% in the case of Terra band 8 near the end of scan.

As a result of these discrepancies, these desert PICS are now used as a reference to calculate the gain of the select RSB, in place of the OBC-based calibration method. For calibration of the gain using the desert PICS, the desert data trends are used to calculate the change in gain on-orbit, with the initial on-orbit SD calibration providing an absolute reference. This is written as

$$\frac{1}{G(t,\theta)} = \left(\frac{m_1(t_0)}{RVS_{prl}(\theta)}\right)\frac{1}{G^{oo}(t,\theta)} \tag{6}$$

where the $G^{oo}(t,\theta)$ is the on-orbit gain change (i.e. normalized to mission start) and $m_1(t_0)$ is measured from the on-orbit solar diffuser calibration at mission start. To calculate the on-orbit change in gain, we rely on the assumption that the normalized reflectance of the desert PICS is constant in time at all AOI, i.e. $\rho(t,\theta) = \rho(0,\theta)$. Then, from Eq. 5 the on-orbit gain change is simply given by

$$G^{oo}(t,\theta) = \frac{dn_2(t,\theta)}{dn_2(0,\theta)} \quad (7)$$

To calculate this gain in practice, we first record the desert dn_2 at each AOI over the entire mission. We then divide the results by the on-orbit change in gain from the OBC-based method, generating trends like those in Figure 3. The purpose of this step is to use the SD and lunar trends to track the short-term and detector-dependent changes in gain, since the OBC data have a better signal-to-noise than the desert data, and then to use the desert data to adjust the long term trend (averaged over all detectors in a band) to the accurate value. These time series are fit in time using a piece-wise polynomial, and then multiplied by the OBC-based gain to restore the full trend. These fitted curves are normalized to mission start and then fit over AOI by either a quadratic or a quartic polynomial, giving a smooth function of the on-orbit gain as a function of AOI and time. Examples of the AOI fitting of the data are shown in Fig. 4. Also plotted are points of the on-orbit gain trends of the lunar-derived gain for comparison.

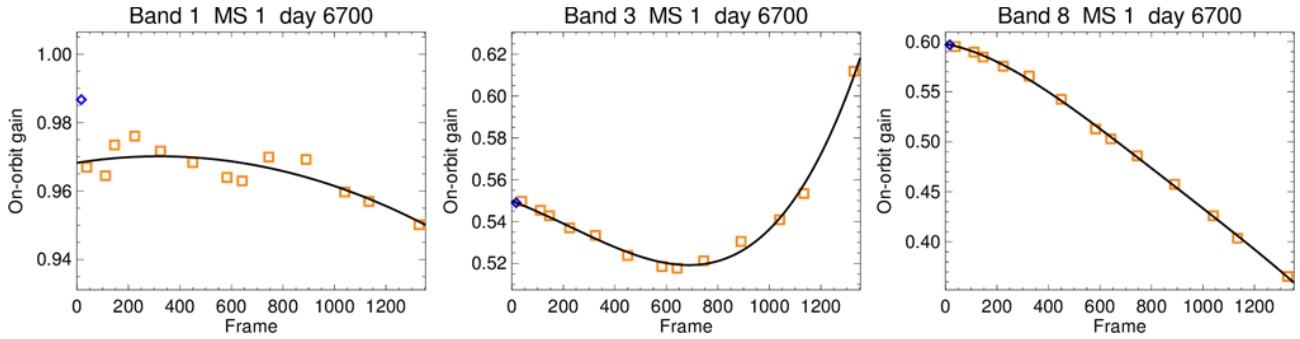

Figure 4. Examples of AOI fitting of the desert data trends for Terra bands 1, 3, and 8, mirror side 1, on day 6700 (May 2018). The blue diamonds mark the value of the on-orbit lunar gain at the same point in time.

Table 2. Summary of the differences in RVS calculations between C6 L1B and C6.1 L1B.

L1B Collection	Initial Date	Bands 1-2	Bands 3-4	Bands 8-9	Band 10
Terra Collection 6	2012-July	EV-based RVS for entire mission	EV-based RVS for entire mission	EV-based RVS for entire mission	OBC-based RVS from mission start to 2014-Feb and EV-based RVS after
Terra Collection 6.1	2017-March	EV-based RVS for entire mission; re-processed results for 2012-Jan through 2017-Feb	EV-based RVS for entire mission	EV-based RVS for entire mission	OBC-based RVS from mission start to 2014-Feb and EV-based RVS after
Aqua Collection 6	2011-Nov	OBC-based RVS from mission start to 2016-July and EV-based RVS after	OBC-based RVS from mission start to 2016-July and EV-based RVS after	EV-based RVS for entire mission	OBC-based RVS for entire mission
Aqua Collection 6.1	2017-Aug	EV-based RVS for entire mission	EV-based RVS for entire mission	EV-based RVS for entire mission	OBC-based RVS for entire mission

As mentioned earlier, the on-orbit gain trends from the lunar calibration agree well with the on-orbit gain trends derived from the desert calibration, with the exception of bands 1 and 2 which show deviations of up to 2.5%. The cause of this deviation is under investigation. One possibility is an on-orbit change in the detector linearity; since the desert sites are brighter than the moon, the two calibrations are performed in different parts of the sensor's dynamic range. We note that bands 1 and 2 also show other unexpected trends, e.g. the gain has increased over the mission (see Fig. 1), and a full understanding of the calibration of these bands has been challenging. For the bands that show good agreement between the lunar and desert trends, the fitting over AOI is constrained to the value of the on-orbit gain of the lunar trend. This

serves to fix the gain at the lunar AOI to the lunar trend, which has higher signal-to-noise than the desert trends. This constraint has only a modest effect on the gain curve at small AOI values, and no real effect for a majority of the AOI curve.

This algorithm is used in both MODIS C6 and C6.1 L1B, and more details can be found in previous reports.[4,9,10] The current MODIS C6 L1B and C6.1 L1B products use the same algorithm for the calculation of m_1/RVS, but the history of the calculation is different for the two collections. Table 2 summarizes the difference between C6 and C6.1 calibration for the MODIS RSB. The initial date indicates the month of LIB LUTs initial delivery for the collection. Prior to this date, the calibration over the entire mission is processed to generate smooth trends in the calibrated gains. After this date, the gains are the results of forward predictions which have been updated on a near-monthly basis. The C6 L1B initially used the OBC-based RVS for Aqua bands 1-4 and later switched to the EV-based RVS in July, 2016. For Terra C6, bands 1-4 used the EV-based RVS for the entire mission, but the results from February, 2012 through the start of C6.1 L1B production for bands 1 and 2 were re-processed to generate a smoother trend that does not carry the errors associated with forward prediction.

4. ALTERNATIVE RVS

The on-orbit gains derived from the desert targets as described above has provided a reliable calibration for the chosen MODIS bands. The calibration has shown generally good agreement with RVS trends calculated from other desert sites and from DCC data, indicating the calibration is accurate. But the desert data have significantly higher noise relative to the on-board calibrators, and we would like to explore variations of the algorithm for calculating a desert-based calibration that could improve upon the accuracy or uncertainty of the current approach used to generate the C6.1 L1B.

An alternative method for calculating the on-orbit change in the RVS was previously presented.[11,12] The alternative algorithm (Alt-RVS) also relies on trends of desert PICS, but with two key differences: (1) it uses data from only one site, Libya 4 (see Table 1), rather than a combination of desert sites, and (2) it derives the on-orbit gain $G^{oo}(t,\theta)$ using the on-orbit lunar gain as a reference, and it uses the desert data only to derive the RVS relative to the lunar AOI. One potential advantage is that this approach allows us to somewhat relax the restriction on the invariability of the desert site.

A major concern in the current C6 calibration approach is the reliance on the long-term calibration stability of the desert PICS, so we seek to reduce the reflectance stability requirement as much as is possible. For the Alt-RVS approach, we consider that the PICS may have a variation in their overall reflectance as a function of time, as long as the angular dependence of the site BRDF remains invariant, i.e.

$$\rho(t,\theta) = f(t)\rho(0,\theta) \tag{8}$$

Since $f(t)$ is unknown, we need another data source to solve for the gain. For this we use the on-orbit lunar calibration trends, and the assumption that the lunar radiance is truly invariant in time. Using this assumption and Eqs. 5, 6, and 8, we write the on-orbit gain change from the desert site as

$$G^{oo}(t,\theta) = G^{oo}_{moon}(t)\,\frac{dn_2(0,\theta_{moon})}{dn_2(t,\theta_{moon})}\frac{dn_2(t,\theta)}{dn_2(0,\theta)} \tag{9}$$

Note that the absolute gain is still based on the initial SD calibration through Eq. 6. Contrasting Eq. 9 with Eq. 7 shows the key difference that normalization to the lunar gain has on the gain calculation for the Alt-RVS vs the C6 method. For the Alt-RVS method it is also important to use data from only one site, since the potential variation of reflectance in time, $f(t)$, could be different for different sites. In the previous presentations of the Alt-RVS method, the order of processing of the desert dn_2 was also done somewhat differently than in the C6 method: the data was fit first over AOI and then over time. But in principle, the method of fitting or simply smoothing the dn_2 data points should not have an impact on the calculated gain, to within the noise of the data. The important differences in the two algorithms are in the input data used (3 sites vs 1 site) and the method of normalization to the lunar gain.

For this paper, we calculate the Alt-RVS gain as follows. The data from all AOI of the Libya 4 site are corrected for background, instrument temperature effects, Earth-Sun distance, cosine of the solar illumination angle, and the BRDF correction just as in the C6 algorithm. We then split the EV data from all frames into monthly bins, and perform a polynomial fit to the data over AOI. Monthly bins are chosen for convenience, but bins with different lengths of time could be used. The results of an example fitting are shown in Fig. 5. Again, we note that the variation in dn_2 with AOI

is partly due to the RVS of the scan mirror and partly due to the differences in site BRDF with AOI that have not been removed.

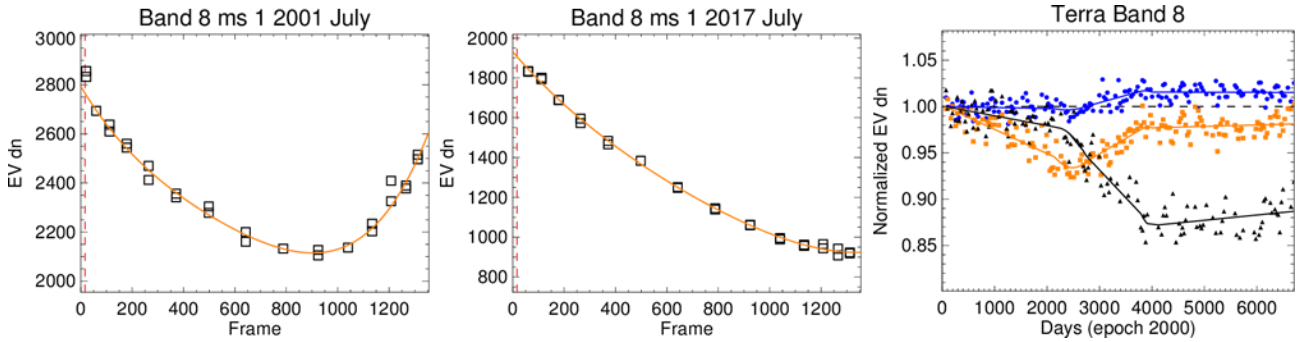

Figure 5. Examples of the AOI and time fitting of the Libya 4 data in the Alt-RVS method for Terra band 8 mirror side 1. The vertical dashed red line in the first two panels indicates frame 17, the AOI of the lunar measurements at which the AOI fit will be normalized. In the right panel, the time trends (relative to the OBC-based gain) are shown for frames 100 (blue circles), 600 (orange squares), and 1100 (black triangles). The time trends can be monitored at any arbitrary AOI since they are based on the AOI fitting result.

The fitted curve as a function of AOI is normalized to the on-orbit lunar gain, giving a set of lunar-normalized curves for every month in the mission. The data are then fit in time with the same process as in the C6 method where the fit is done relative to the OBC-based gain. Examples of the time fitting (relative to the OBC-based gain) are shown in Fig. 5. Finally, the results of the time fitting are fit again over AOI in order to get the coefficients that are used in the L1B LUTs.

5. RESULTS AND DISCUSSION

5.1 Comparison of C6 and Alternative RVS results

Figure 6 shows a comparison of the absolute inverse gain (m_1/RVS) for bands 1-4, and 8 over the Aqua MODIS mission for both the C6 and the Alt-RVS calculations, as well as the relative difference between the results. For bands 1 and 2, there is a clear divergence between the two methods in the overall gain for most AOI of up to 2% over the mission. This is due to the previously known divergence between the lunar trend and the desert trends at the lunar AOI. In the C6 method, the lunar data is ignored, but in the Alt-RVS method, the entire desert data set is normalized to the lunar gain, so the difference is transferred to all AOI. For bands 3, 4, and 8, the results from the two methods are within 1% of each other except for a few frames of band 3 late in the mission. Figure 7 shows the results comparison for Terra MODIS. As with Aqua, bands 1 and 2 show a divergence in the overall gain over the mission for the same reason. For bands 3, 4, and 8, the two methods differ by up to 2%, a somewhat larger difference than is seen in Aqua MODIS. We did not evaluate the Alt-RVS method for band 10 of Terra MODIS, since the Libya 4 site is saturated in the early part of the mission. We also leave out the Alt-RVS results for Terra and Aqua band 9, which we discuss later.

5.2 Uncertainty comparison

Before considering the difference between the two methods in more detail, we first discuss an uncertainty comparison. The method used for calculating the uncertainties of the EV reflectance using the C6 method of PICS-based calibration was recently presented in detail.[17] In brief, we determine the fitting residuals of the two-step fitting process of the corrected EV data (time fitting followed by AOI fitting) as a function of time using yearly averaged values, and then combine the two to get a total fitting uncertainty that represents the typical noise of the data for each AOI. These uncertainty values are then fit over AOI to get uncertainty at the 7 frames of the C6/6.1 L1B uncertainty index. The results are shown in Figure 8 for Terra bands 3, 4, and 8. At the lunar frame, the uncertainty is taken to be the uncertainty in the lunar calibration, rather than the EV-based gain. Note that the uncertainty in Fig. 8 is just the uncertainty in deriving the time-dependent on-orbit gain. The complete uncertainty of the EV reflectance product includes other terms, such as scene-dependent noise and pre-launch calibration uncertainties, which are not shown here.

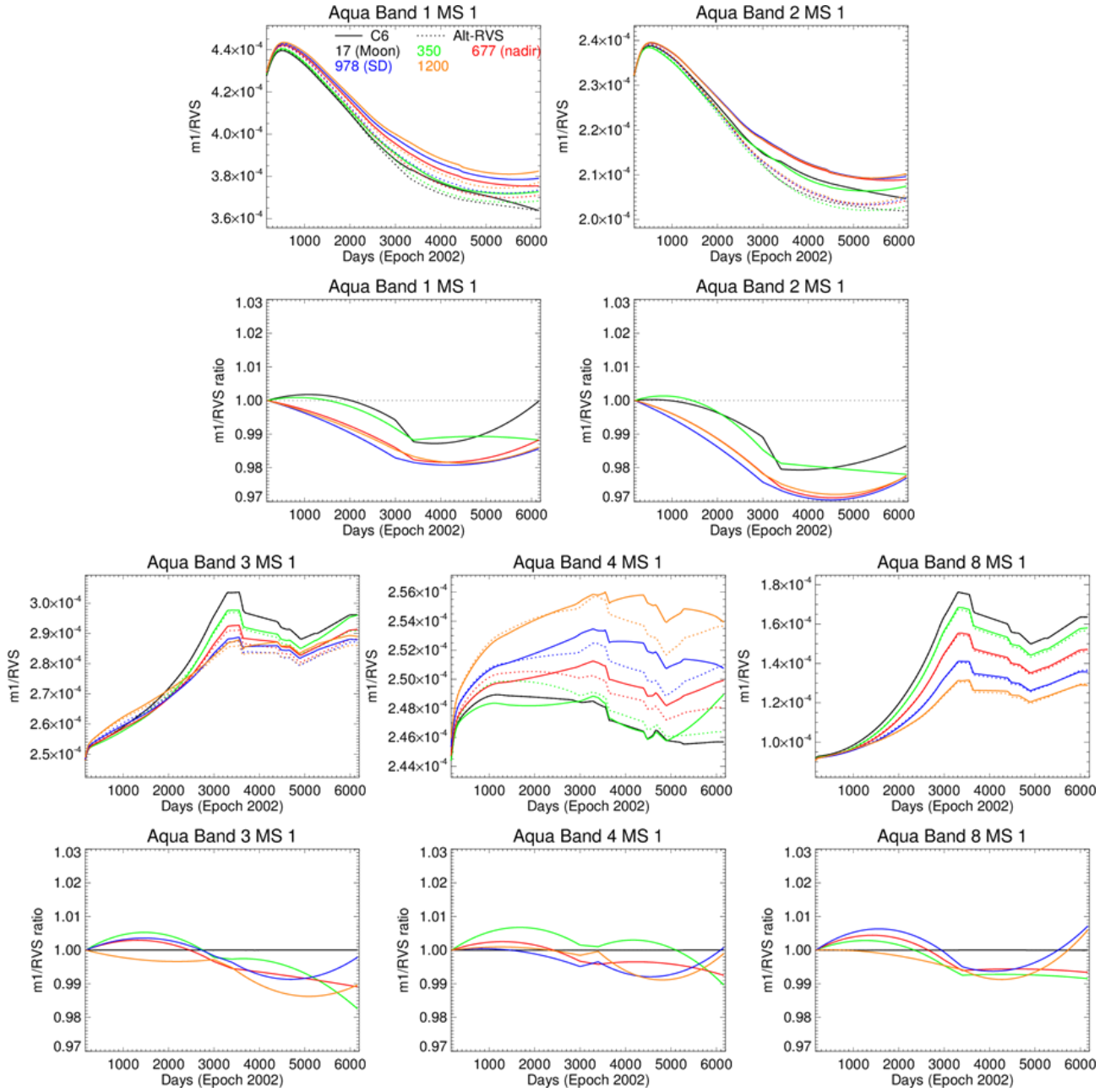

Figure 6. Comparison of the inverse gain trends for Aqua MODIS for the C6 vs Alt-RVS calculations. Results are shown for mirror side 1 for bands 1, 2, 3, 4, and 8. The results for mirror side 2 are similar.

For the Alt-RVS method, we use the same strategy of simply calculating the fitting residuals of the two-step fitting (AOI fitting followed by time fitting). The results are also shown in Figure 8. The Alt-RVS method has slightly higher values, but the results are generally in agreement with each other, as expected, since the three desert sites have similar noise and the order of fitting should not have a major impact on the overall fitting residuals. The results for Aqua MODIS (not shown) have slightly lower uncertainty in general, but the differences between bands and methods are similar to that seen in Terra.

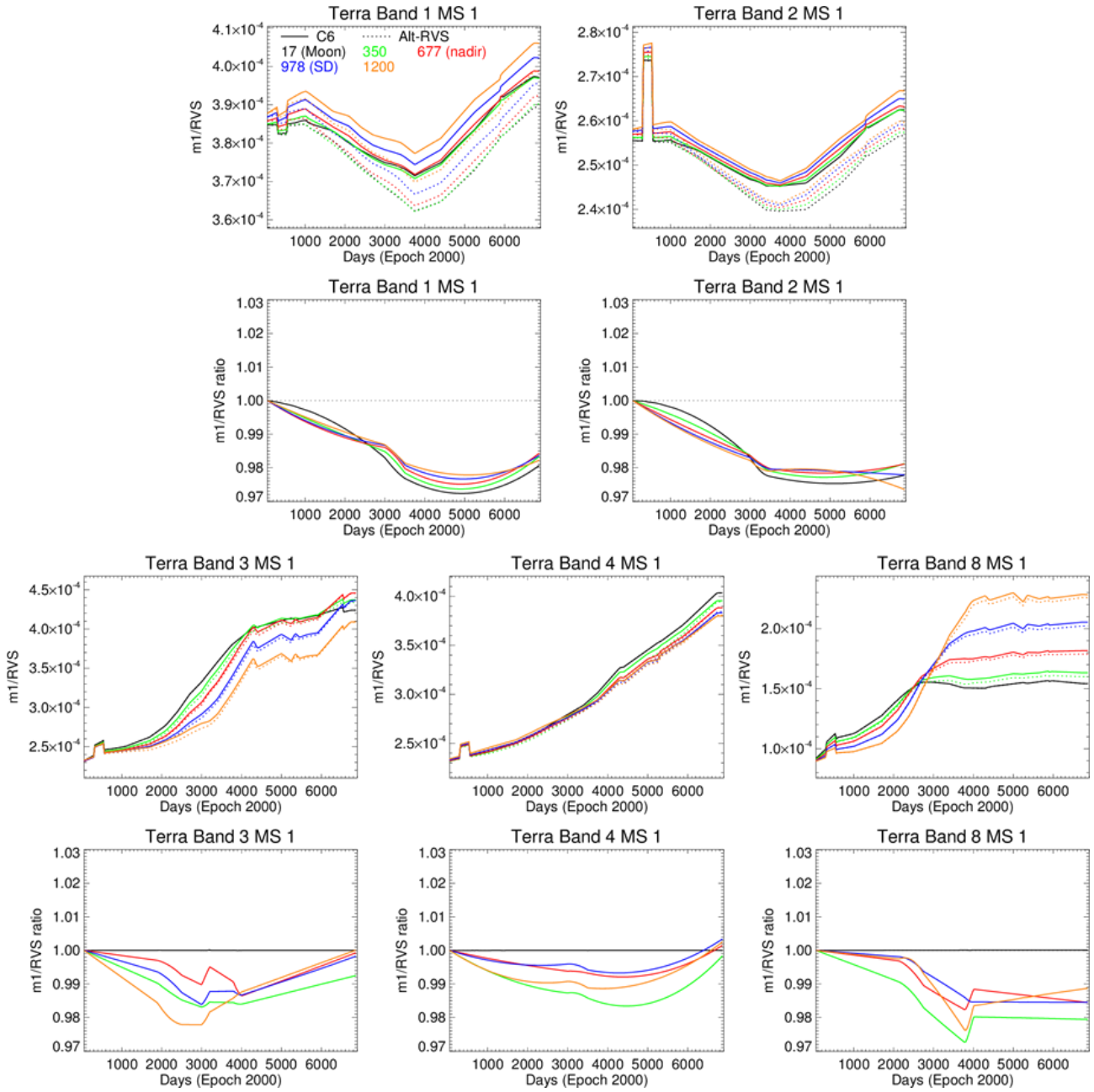

Figure 7. Comparison of the inverse gain trends for Terra MODIS for the C6 vs Alt-RVS calculations. Results are shown for mirror side 1 for bands 1, 2, 3, 4, and 8. The results for mirror side 2 are similar.

5.3 Uncertainty due to lunar normalization

The simple uncertainty method just described leaves out at least one important consideration. A key difference in the two methods is that the Alt-RVS method normalizes the EV dn to the lunar frame. This normalization to the lunar frame means that the overall calibrated gain (m_1) is dependent on the accuracy of the fitted EV dn at the lunar AOI, which is very near the edge of the scan (beginning of scan). As can be seen in Fig. 2, the AOIs near the edge of scan have much larger BRDF impact that those near nadir, which can certainly affect the precision of the results. Especially for the blue bands, Rayleigh-scattered light will increase the signal observed farther from nadir and this is very likely the main reason that the corrected dn moves sharply upward toward the edges of scan (see Fig. 5). Changes in the amount of Rayleigh-scattered light with time represent a possible systematic uncertainty in the EV trends near the scan edges, even

if the desert reflectance at the surface is perfectly stable. Also, any unconstrained polynomial fit will have larger uncertainty in the fitted values near the edges of the fit. As can be seen from Fig. 5, the shape of the EV dn is much sharper at the edges of the scan than it is at nadir and the tail of the quartic fit can be significantly changed by small variations in points either at the beginning or at the end of scan.

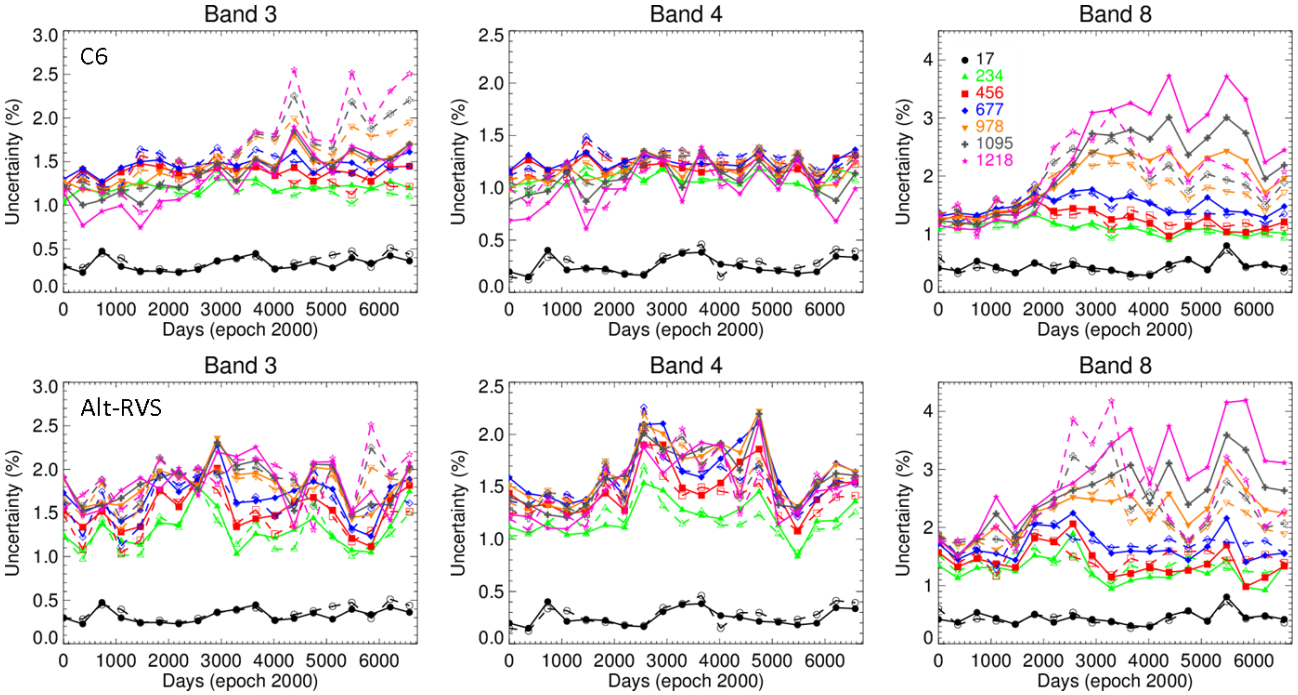

Figure 8. Time-dependent uncertainty for Terra bands 3, 4, and 8 using the C6 (top row) and Alt-RVS (bottom row) algorithms. Solid lines and filled symbols represent mirror side 1 results and dashed lines and open symbols represent mirror side 2 results. The legend in the upper right indicates the frames at which uncertainty is calculated, including the lunar (17), nadir (677) and SD (978).

As an example of this, consider the case of Terra band 8, which had the largest disagreement between the C6 and Alt-RVS methods in Fig 7. All frames greater than 300 diverge in nearly the same way, suggesting that the RVS between the two methods is the same except for the first 300 frames. The Alt-RVS error in the early frames may be partly due to the initial AOI fitting (Fig. 5) systematically underestimating the dn at the lowest frames. But because the Alt-RVS method normalizes the gain to the lunar frame, any error in the RVS fitting at small AOI is transferred to all AOI. Similarly, band 9 of both Aqua and Terra has some saturation problems at small AOI early in the mission. The lack of data at small AOI makes the AOI fit result in this region more uncertain, and thus the Alt-RVS gain trends for band 9 can vary greatly with small changes in the fitting strategy, which is not ideal. Since the calibration accuracy near nadir is more important than the accuracy at beginning or end of scan, normalizing the calibration data to a point very near the beginning of scan may be counterproductive, unless there is strong evidence (which we have not yet seen) that indicates the stability of the near-nadir desert trends is unreliable.

5.4 Other considerations

In all of this analysis, we have used the BRDF-corrected desert data, dn_2. But we can also consider analyzing the uncorrected data directly. The effect of the site BRDF is to cause yearly oscillations in the response, but it does not impact the multi-year trend. If the results are fit over time using only data from similar times of the year, e.g. only data from the month of July as was done in Chen et. al., 2016, then the long term trends can be derived without the need for BRDF correction. This idea could be applied to either the C6 or Alt-RVS calibration method. While this idea provides some simplification, it makes it more difficult to monitor short term changes in the instrument and provide accurate forward predictions while the MODIS data collection is still on-going.

When the Terra and Aqua satellites approach end of life, the MODIS instruments may be required to maintain calibration during a de-orbiting phase. In this scenario, the repeatable 16-day cycle for observations of desert PICS at

the same AOI will not be maintained, and viewings at other AOI will become available. The current method separating the data into specific AOI time series and deriving a BRDF correction separately for each AOI time series will necessarily have to be re-examined, and an RVS calibration based on a single site may be more attractive.

6. CONCLUSION

We have reviewed the on-orbit calibration algorithms for the RSB of Terra and Aqua MODIS. Two distinct methods for calibrating the gain of select RSB using a combination of lunar calibrations and pseudo-invariant desert targets were examined. The Alt-RVS method can provide an accurate calibration of the MODIS RSB and shows reasonably good agreement with the well-tested method currently used in the C6/C6.1 L1B, particularly for Aqua MODIS. The Alt-RVS method has the advantage of a less stringent requirement on the temporal stability of the reference PICS. However, the process of normalization of gain to the lunar AOI creates an increased possibility of introducing systematic errors, due to the difficulty in fitting and/or properly modeling the EV data at the edges of scan, particularly for the short wavelength bands where Rayleigh scattering has a significant impact. In light of this, the current C6 approach is likely a more reliable choice, as long as deviations between the desert and lunar trends are closely monitored and understood. We have focused on these two methods in this paper since the algorithms have been previously published, but of course there is a continuum of ways to analyze the data from the desert PICS to derive MODIS RSB gains. The MODIS Characterization Support Team (MCST) will continue to explore methods of Earth-based calibration using the desert PICS and other Earth targets with the goal of providing an accurate calibration with the lowest uncertainty possible.

ACKNOWLEDGEMENTS

We thank other past and present members of MCST for their work developing the algorithms for RSB calibration, and we thank Dr. Tiejun Chang for providing a technical review of this paper.

REFERENCES

[1] Xiong, X., Sun, J., Xie, X., Barnes, W. L. and Salomonson, V. V., "On-Orbit Calibration and Performance of Aqua MODIS Reflective Solar Bands," IEEE Trans. Geosci. Remote Sens. **48**(1), 535–546 (2010).

[2] Xiong, X., Sun, J., Barnes, W., Salomonson, V., Esposito, J., Erives, H. and Guenther, B., "Multiyear On-Orbit Calibration and Performance of Terra MODIS Reflective Solar Bands," IEEE Trans. Geosci. Remote Sens. **45**(4), 879–889 (2007).

[3] Angal, A., Xiong, X., Wu, A., Chen, H., Geng, X., Link, D., Li, Y., Wald, A. and Brinkmann, J., "On-orbit performance and calibration improvements for the reflective solar bands of Terra and Aqua MODIS," Proc. SPIE **9881**, 98811F (2016).

[4] Sun, J., Xiong, X., Angal, A., Chen, H., Wu, A. and Geng, X., "Time-Dependent Response Versus Scan Angle for MODIS Reflective Solar Bands," IEEE Trans. Geosci. Remote Sens. **52**(6), 3159–3174 (2014).

[5] Sun, J.-Q., Xiong, X., Barnes, W. L. and Guenther, B., "MODIS Reflective Solar Bands On-Orbit Lunar Calibration," IEEE Trans. Geosci. Remote Sens. **45**(7), 2383–2393 (2007).

[6] Pan, C., Xiong, J. and Che, N., "MODIS pre-launch reflective solar band response vs. scan angle," Proc. SPIE **6677**, 66770R (2007).

[7] Sun, J., Xiong, X., Chen, H., Angal, A., Geng, X. and Wu, A., "Time-dependent response versus scan angle for MODIS reflective solar bands," Proc. SPIE **7452**, 745219 (2009).

[8] Sun, J., Xiong, X., Angal, A., Chen, H., Geng, X. and Wu, A., "On-orbit performance of the MODIS reflective solar bands time-dependent response versus scan angle algorithm," Proc. SPIE **8510**, 85100J (2012).

[9] Geng, X., Angal, A., Sun, J., Chen, H., Wu, A., Li, Y., Link, D. and Xiong, X., "Status of time-dependent response versus scan-angle (RVS) for Terra and Aqua MODIS reflective solar bands," Proc. SPIE **9218**, 92181P (2014).

[10] Angal, A., Xiong, X., Wu, A., Geng, X. and Chen, H., "Improvements in the On-Orbit Response Versus Scan Angle Characterization of the Aqua MODIS Reflective Solar Bands," IEEE Trans. Geosci. Remote Sens. **56**(3), 1728–1738 (2018).

[11] Chen, H., Xiong, X. and Wu, A., "Alternative approach to characterize response versus scan-angle (RVS) for MODIS reflective solar bands," Proc. SPIE **8176**, 817612 (2011).
[12] Chen, H., Xiong, X., Angal, A., Geng, X. and Wu, A., "Alternative method of on-orbit response-versus-scan-angle characterization for MODIS reflective solar bands," J. Appl. Remote Sens. **10**(2), 024004 (2016).
[13] Angal, A., Xiong, X., Mu, Q., Doelling, D. R., Bhatt, R. and Wu, A., "Results From the Deep Convective Clouds-Based Response Versus Scan-Angle Characterization for the MODIS Reflective Solar Bands," IEEE Trans. Geosci. Remote Sens. **56**(2), 1115–1128 (2018).
[14] Bhatt, R., Doelling, D. R., Angal, A., Xiong, X., Scarino, B., Gopalan, A., Haney, C. and Wu, A., "Characterizing response versus scan-angle for MODIS reflective solar bands using deep convective clouds," J. Appl. Remote Sens. **11**(1), 016014 (2017).
[15] Mu, Q., Wu, A., Xiong, X., Doelling, D., Angal, A., Chang, T. and Bhatt, R., "Optimization of a Deep Convective Cloud Technique in Evaluating the Long-Term Radiometric Stability of MODIS Reflective Solar Bands," Remote Sens. **9**(6), 535 (2017).
[16] Roujean, J.-L., Leroy, M. and Deschamps, P.-Y., "A bidirectional reflectance model of the Earth's surface for the correction of remote sensing data," J. Geophys. Res. **97**(D18), 20455 (1992).
[17] Xiong, X., Angal, A., Barnes, W. L., Chen, H., Chiang, V., Geng, X., Li, Y., Twedt, K., Wang, Z., Wilson, T. and Wu, A., "Updates of Moderate Resolution Imaging Spectroradiometer on-orbit calibration uncertainty assessments," J. Appl. Remote Sens. **12**(03), 1 (2018).